Antarctic climate change over the twenty first century

Thomas J. Bracegirdle*, William M. Connolley, John Turner

British Antarctic Survey, Cambridge, UK

Submitted to Journal of Geophysical Research

24 October 2007

Running title: 21st century Antarctic climate change

*Corresponding author address (responsible for checking proofs):
British Antarctic Survey, Cambridge, CB3 0ET, UK
e-mail: tjbra@bas.ac.uk
tel: +44 (0) 1223 221571
fax: +44 (0) 1223 362616

Abstract

Here we present a new assessment of Antarctic climate change over the 21st century based on data from the models that were developed as part of the Intergovernmental Panel on Climate Change (IPCC) 4th Assessment Report (AR4). To provide more reliable estimates of future change, a weighting scheme was applied to the model output, which depends on a measure of their ability to reproduce the mean climate of the late 20th century. The results show a seasonal variation of increases in circumpolar westerlies around Antarctica, which show the largest increases of 27% in autumn. This seasonal cycle was found to be consistent with projected changes in the semi-annual oscillation (SAO). In summer and autumn the increases of the westerly wind component migrate sufficiently far south to be manifested as a reduction of the coastal easterlies. The surface warming averaged over the continent is projected to be 0.34°C dec^{-1} with an inter-model standard deviation of 0.10°C dec^{-1}. More rapid warming occurs during the winter over regions of sea ice retreat, e.g. 0.51 ± 0.26°C dec^{-1} around East Antarctica. Projections of total sea-ice area show a decrease of 2.6 ± 0.73 × 10^{6} km^{2} (33%). There is a projected increase of net precipitation averaged over the continent of 2.9 ± 1.2 mm a^{-1} dec^{-1}. The weighting gives a larger increase of the autumn SAO peak, up to 30% larger for April. This is consistent with larger weighted autumn increases of circumpolar westerlies, more sea ice reduction and resulting larger skin temperature increases.

1. Introduction

Robust regional changes in future global warming scenarios, such as increases of high-latitude precipitation, and advances in climate model simulations of recent regional climate change, such as the winter warming of the Antarctic Peninsula [*Carril et al.*, 2005], have increased the confidence in regional climate projections of the future. However, some models still produce output with large regional differences from observations. For instance, *Miller et al.* [2006] found a large inter-model spread of an index of the southern annular mode (SAM) in both current and future climate simulations of 14 different coupled climate models. Previous studies have found that by weighting individual members of a model ensemble according to some measure of their performance, the spread of projections can be reduced and/or the ensemble mean changed when compared to statistics without model weighting [*Murphy et al.*, 2004; *Tebaldi et al.*, 2004; *Schmittner et al.*, 2005]. In addition, *Räisänen* [2007] showed evidence for a relationship between simulated present-day high-latitude climate bias and future change. Here future projections contributed by various modeling groups to the Intergovernmental Panel on Climate Change (IPCC) 4th Assessment Report (AR4) were weighted as described by *Connolley and Bracegirdle* [2007], who assigned weights based primarily on model performance at high southern latitudes.

Data from 24 climate models are available as part of the AR4 effort and form the World Climate Research Programme's (WCRP's) Coupled Model Inter-comparison Project phase 3 (CMIP3) multi-model data set. The following studies of 21st century climate evolution over Antarctica are based on the CMIP3 data set. The CMIP3 models indicate that the current maximum of warming over the Antarctic Peninsula will not continue into the future [*Carril et al.*, 2005]. The warming is projected to become more uniform over the continent, with the largest annual average increases over the high altitude interior and the Weddell Sea region. Increased warming off the coast of Antarctica is associated with the projected reduction of sea ice extent of approximately 25% by the end of the 21st century [*Arzel et al.*, 2006]. The larger moisture capacity of the atmosphere in a warmer climate and a poleward migration of the mid-latitude cyclone track contribute to projected increases of the annual precipitation over the 21st century [*Lynch et al.*, 2006; *Lambert and Fyfe*, 2006]. The simulated increase of precipitation rate leads to an increase of accumulation of mass over Antarctica [*Gregory and Huybrechts*, 2006] and a negative contribution to sea level rise.

Large-scale patterns of climate variability play a key role in understanding the regional aspects of both the projected climate changes described above and observed past changes [*van den Broeke*, 1998; *Marshall*, 2007] , thus motivating assessment of the evolution of known patterns of variability over the 21st century. Many analyses of the response of the SAM to changes in key climate forcing factors have been conducted [e.g., *Shindell and Schmidt*, 2004; *Carril et al.*, 2005; *Miller et al.*, 2006]. However, little attention has been given to the role of the semi-annual oscillation (SAO) in interpreting the characteristics of 21st century climate change. This is partly due the difficulty that many models have in simulating the observed spring peak in the SAO, which has been attributed to a poor representation of the annual cycle of mid-latitude tropospheric temperatures [*Raphael and Holland*, 2006]. Given such challenges in the simulation of patterns of variability around Antarctica and their

important role for understanding future change, parameters that both describe and affect the SAM and SAO were used (where reliable observation-based data are available) in the weighting scheme of *Connolley and Bracegirdle* [2007].

There are three key aims to this study. Firstly the assessment of 21st century atmospheric circulation changes associated with the SAM and SAO. Secondly the application of a weighting scheme to projections of key climate variables over Antarctica. Thirdly to present a broad and more comprehensive perspective of Antarctic climate change, since previous studies have mainly focused on one aspect of future Antarctic climate change making it difficult to build a comprehensive picture of Antarctic climate evolution over the 21st century from any one paper.

This paper is structured as follows. The data and methods are described in the next section. Projected 21st century changes to large-scale atmospheric circulation patterns are shown in section 3 followed by an assessment of changes to near-surface winds, sea ice, temperature and net precipitation in section 4. The discussion and conclusions are in section 5.

2. Data and methods

In this study the World Climate Research Programme's (WCRP's) Coupled Model Inter-comparison Project phase 3 (CMIP3) multi-model data set was used. This data set was compiled primarily for the IPCC AR4. Model data were retrieved from the data portal at https://esg.llnl.gov:8443/, from which 19 of the 24 available models were found to have the data required for this assessment (Table 1). The CMIP3 models are coupled ocean/atmosphere/sea-ice models with factors important for climate forcing prescribed according to different scenarios. The experiments used in this study are the '20C3M' climate of the 20th century experiment and the Special Report on Emissions Scenarios (SRES) A1B future climate change scenario. The SRES A1B scenario was chosen since the largest number of models provided required data for analysis of this scenario. In terms of global temperature, the SRES A1B scenario is about the middle of the range of changes projected by the different SRES scenarios. It is not considered to be more or less likely than other SRES scenarios. The SRES A1B runs were started from the end of the 20C3M runs at around the year 2000.

The CMIP3 simulations were run using prescribed concentrations of long-lived greenhouse gases (GHGs), CO_2, CH_4 and N_2O. The 20C3M runs were forced with observed long-lived (GHG) concentrations and span a period from the mid 19th century to the end of the 20th century. The long-lived GHG concentrations in the future scenarios were estimated from projected changes to energy use, industry and land use. For the SRES A1B future scenario, concentrations of CO_2 are projected to reach 720 ppm in the year 2100. For both the 20C3M and SRES A1B runs the sulfate aerosol concentrations were calculated from prescribed sulfur dioxide (SO_2) emissions, but vary between models due to different methods of calculation. Both sets of runs also include inter-model differences of forcing by stratospheric ozone and volcanic aerosols, which are important for the Southern Hemisphere circulation due their role in long-term changes of the southern annular mode (SAM) [*Shindell and Schmidt*, 2004; *Miller et al.*, 2006]. For the SRES A1B scenario, most models were run with a gradual recovery of stratospheric ozone to pre-industrial levels over the 21st

century, but some did not include any stratospheric ozone forcing [see *Miller et al.*, 2006].

Model data from the '20C3M' experiment, that was designed to simulate observed climate evolution over the 20th century, were used to weight the models according to their level of agreement with observations of climate in the late 20th century. The weighting methodology used by *Connolley and Bracegirdle* [2007] is largely based on that of *Murphy et al.* [2004] and *Schmittner et al.* [2005]. The weights assigned to each model are shown in Table 1. The weighting was constructed from observation-based estimates of the following parameters: mean sea level pressure (MSLP), 500 hPa geopotential height, sea surface temperature (SST), 500 hPa temperature and precipitation minus evaporation (P-E). These parameters were assessed both globally and over southern high latitudes (south of 45°S), apart from P E, for which reliable estimates exist over the Antarctic continent, but is difficult to calculate accurately away from perennially frozen surfaces over land. Global errors were taken into account because, although this analysis is focused on Antarctica, global processes are important for the Antarctic through factors such as ocean heat transport and atmospheric teleconnection patterns.

For mean sea level pressure (MSLP), the observation-based data used were taken from ERA40 [*Uppala et al.*, 2005]. MSLP is effectively a fictitious quantity over regions of high altitude orography and was therefore assessed for regions with orography below an altitude of 100 meters above mean sea level. For 500 hPa temperature and geopotential height, ERA40 data were also used. Data from the Goddard Institute for Space Studies (GISS) models EH and ER had very large values in these fields in a small region over the high altitude orography of the Himalayas; the affected data were replaced by climatological ERA40 data. For sea surface temperature, the GISS surface temperature analysis observational data were used. Surface temperatures over the Antarctic continent and sea ice zone were not assessed due to sparse observations and poor performance of reanalysis products [*Connolley and Harangozo*, 2001]. For P-E over the Antarctic continent the surface mass balance analysis of *Vaughan et al.* [1999] was used.

3. Large-scale patterns of variability

3.1. The SAM

The projected strengthening and southward migration of the circumpolar westerlies in the Southern Hemisphere [see *Fyfe and Saenko*, 2006] is associated with an increasingly positive SAM over the 21st century [*Miller et al.*, 2006]. Climate models exhibit a more positive SAM in all seasons in response to increases of GHG concentrations [*Shindell and Schmidt*, 2004]. Over the first half of the 21st century the simulated response of the SAM to increasing GHGs is offset in summer by the recovery of stratospheric ozone concentrations [*Miller et al.*, 2006].

Annular increases of the circumpolar westerlies associated with SAM increases are evident in Figure 1. Over the next 100 years the seasonal ensemble mean changes of the SAM (according to the index of *Gong and Wang* [1999] without their normalization, i.e. the zonally averaged difference between MSLP at 40S and 65S) are 2.7, 3.8, 4.8 and 3.1 hPa for summer, autumn, winter and spring respectively. This

contrasts with the projected changes of the westerlies around Antarctica (~60S), which show peak increases of the westerly wind component in autumn and little difference between winter and summer. The seasonal cycle of these more regional changes is suggestive of a change in the SAO.

3.2. The SAO

The semi-annual oscillation (SAO) is manifested in sea-level pressure (SLP) as a twice-yearly expansion and contraction of the circumpolar trough at high southern latitudes. The expansion and weakening phases last from March to June and September to December and the contraction and strengthening phases last from June to September and December to March. These twice-yearly expansion (contraction) phases in SLP are associated with weakening (strengthening) phases of the mid-tropospheric meridional temperature gradient in the sub-Antarctic region [*van Loon*, 1967]. These changes of the temperature gradient are a result of different annual cycles of tropospheric temperature over Antarctica (~65S) and further north over the open ocean (~50S). The larger heat capacity of the ocean at 50S compared to the frozen surface over Antarctica contributes to a lag of the autumn cooling at 50S behind cooling at 65S. However, spring warming at 65S lags that at 50S due to the persistence of what is termed the coreless winter, during which there is no strong temperature minimum during the winter months over the Antarctic continent and spring warming occurs in late August. This, in combination with similar amplitudes of the seasonal temperature cycle at 50S and 65S, results in a twice-yearly increase of the meridional temperature gradient between these two latitudes (e.g. see Figure 4a of *Meehl* [1991]). For both zonally averaged 500 hPa temperature (T500) and SLP the semi-annual cycles of the difference between 50S and 65S are used as an index of the SAO [*van Loon*, 1967; *Meehl et al.*, 1998; *Raphael and Holland*, 2006].

Climatological changes of the SAO have shown a strong link between meridional gradients of SLP and T500. A significant weakening of the amplitude of the SAO occurred in the late 1970s, with largely consistent seasonally varying changes to meridional gradients of both T500 and SLP [*Meehl et al.*,1998]. Modeling studies have also shown a strong link between the meridional gradient of mid-tropospheric temperature and the strength and location of the circumpolar trough [*Meehl*, 1987; *Thompson and Solomon*, 2002].

The CMIP3 models successfully simulate the autumn peak in the SAO, but produce a smaller than observed spring peak [*Raphael and Holland*, 2006]. *Raphael and Holland* [2006] suggested that one reason for the poor simulation of the spring peak is that the models do not correctly simulate the temperature oscillation at 50S. The application of the weighting scheme was found to make little difference to the ensemble average SAO indices. Therefore projections of the spring peak of the SAO should be treated with caution.

Projected 21st century changes to the SLP and T500 gradients in the CMIP3 models influence the SAO. In Figure 2 and Figure 3 the weighted ensemble average SLP and T500 SAO indices at the beginning and end of the 21st century are compared. The SLP SAO index shows a strong semi-annual cycle in most of the CMIP3 models. However, as found for the five models assessed by *Raphael and Holland* [2006], many of the models do not show the observed spring maximum of the T500 SAO

index. The annual cycle of the projected changes to these indices are broadly similar (Figure 2b and Figure 3b), with both exhibiting a maximum change in autumn and a minimum in late winter/spring. However, two key differences emphasize that the changes to the SLP index cannot be explained by the T500 gradient alone. Firstly there is a year-round increase of the ensemble-mean SLP index, whereas the ensemble-mean T500 index does not show increases for September. Secondly the annual cycle of changes of the SLP index lag the changes of the T500 index by approximately two months. Other factors that can affect the SLP gradient in this region are static stability (through its effect on cyclone intensification), SST, greenhouse gases and stratospheric ozone [*Thompson and Solomon*, 2002; *Shindell and Schmidt*, 2004; *Frierson*, 2006; *Marshall*, 2007].

The GFDL CM2.1 model produces a spring peak of the T500 SAO index that is similar in amplitude to observations (see Figure 3 of *Raphael and Holland* [2006]). This model produces projected changes that are similar to the CMIP3 ensemble average in amplitude, but with a slightly different phase. For the SLP SAO index the peak change simulated by GFDL CM2.1 is one month earlier than the CMIP3 ensemble average (February), but the minimum is not different from the ensemble average (October). For the T500 SAO index the peak change simulated by GFDL CM2.1 is two months earlier than the CMIP3 ensemble average (January) and the minimum is about one month earlier (August).

The autumn peak of increases of the T500 gradient between 50S and 65S are part of a meridional migration of increases that are apparent throughout the year (Figure 4). From June to December the largest T500 gradient increases move north to ~35S. This leads to an annual cycle of tropospheric warming at 50S that is much larger than the annual variation of warming at 65S (Figure 5). The increases of the T500 gradient are associated with a poleward shift of the mid-latitude southern hemisphere storm tracks, which is a robust characteristic of future scenarios in the CMIP3 models [*Yin*, 2005]. Static stability is also important to the intensification of baroclinic cyclones. However, *Yin* [2005] found that the poleward shift of a theoretical baroclinic eddy growth rate (the maximum Eady growth rate) is dominated by changes of meridional tropospheric temperature gradient.

The change in the T500 gradient is consistent with a link to changes of the skin temperature gradient (Figure 6). During the late winter/spring the retreat of sea ice causes large reductions of the meridional surface temperature gradient within the latitude range of the SAO (50 to 65°S). These near-surface increases are larger than those at 500 hPa since the warming due to sea ice retreat is largely restricted to the lower troposphere [*Frierson*, 2006]. From the CMIP model output it is not possible to quantify extent to which this surface warming impacts on the mid-troposphere and other factors may also contribute. During the late summer/autumn, there is an increase of the sea surface temperature (SST) gradients centered just north of and extending across the SAO latitude range. This is of a similar magnitude to the increase of the T500 gradient shown in this region in Figure 4a.

The autumn increase of the T500 SAO index projected by the CMIP3 models is similar in magnitude to the observed decrease of the amplitude of the SAO index in the late 1970s [*Meehl et al.*, 1998], but with a different annual variation. The annual variation of the changes of both the T500 and SLP gradients show a more pronounced

strengthening of the autumn peak of the SAO compared to the spring peak. This is manifested in the near-surface winds as a strong autumn contraction and intensification of the circumpolar westerlies around Antarctica (Figure 1).

The largest differences between the weighted and unweighted ensemble projections of the SLP and T500 SAO indices are in the autumn. For April the 21st century increases of the MSLP and T500 gradients are 27% and 30% larger respectively, which in both cases is approximately half of one standard deviation of the inter-model spread (Figure 2(b) and Figure 3(b)). This difference between the weighted and unweighted gradient is mainly due to a more rapid 500 hPa warming (Figure 6) and pressure increases at 50S compared to 65S (not shown). From Figure 4 it is evident that increases of the T500 gradient at lower latitudes (~35S) are also larger in the weighted ensemble mean.

Although weighting the model projections changes the ensemble mean of the SAO indices, there is little difference between the weighted and unweighted inter-model spread of projections of the SLP and T500 gradient SAO indices (Figure 2and Figure 3).

4. Projected changes to key parameters

4.1. Near-surface winds over Antarctica

The near-surface (10m) winds over Antarctica are important for a number of reasons. They are an important influence on sea-ice formation when cold air outbreaks spread over the relatively warm open ocean. The circumpolar westerlies over the Southern Ocean drive the exchange of heat, moisture and momentum. There is also a small effect on the Antarctic mass balance through wind-induced transport of snow into the sea, which contributes to 10% of the removal of the net water input [*Giovinetto et al.*, 1992]. Changes of the near-surface wind speed therefore have implications for the link between atmospheric circulation and other components of the climate system.

Monthly mean data from 15 of the 19 weighted models were found for assessment of the near-surface (10m) winds (Table 1). Results shown in Figure 7 are the magnitude of the monthly-mean 10-meter wind vector, for which changes of magnitude are nearly equivalent to changes of the mean wind speed if the directional constancy (ratio of the average wind vector to the average wind speed) is large. Over the steep orography of the Antarctic continent the directional constancy is very large [*van den Broeke et al.*, 1997]. Over the ocean around Antarctica the directional constancy is small and changes of the mean wind speed will in general differ from monthly-mean wind vector magnitude.

The annual and zonal mean circumpolar westerlies at 60S are projected to increase by 0.73 ± 0.36 m s^{-1} (21 ± 10 %) over the 21st century (here and in the rest of the paper the inter-model spread is expressed as the standard deviation of the projections from different models). The magnitude of the autumn maximum of wind increases at 60S apparent from Figure 1 is 1.13 ± 0.49 m s^{-1} (27 ± 12%). The poleward shift and increases of the westerly wind component result in decreases of the coastal easterlies around Antarctica in summer and autumn, but do not penetrate sufficiently far south

to influence coastal Antarctica in winter and spring (Figure 1 and Figure 7). There is a strong consensus between the models for a decrease of the coastal easterlies, but with a smaller magnitude and less inter-model consensus in the projected decreases over East Antarctica for the unweighted ensemble (Table 2 and Table 3). The weighted ensemble mean trends agree qualitatively with the results of *van den Broeke et al.* [1997], who also found wind speed decreases along coastal East and West Antarctica mainly in summer. The average wind vector magnitude trend over the interior of Antarctica is close to zero, with cancellation between regions of increase and decrease. The increases (up to 10% in autumn) consistently occur in a region that extends over Queen Mary Land and Wilkes Land.

Since summer trends of sea-level-pressure-based SAM indices have been found in climate models to be sensitive to stratospheric ozone concentration [*Shindell and Schmidt*, 2004], the omission of 21st century stratospheric ozone recovery in some of the CMIP3 models is likely to have an impact on the near-surface wind projections in those seasons. However, most of the strongly weighted models include stratospheric 21st century stratospheric ozone recovery. From the 15 models used for the near-surface wind projections, only one (CCCMA CGCM3) out of the five most strongly weighted models omits stratospheric ozone recovery, whereas four out of the five most weakly weighted models omit recovery.

4.2. Sea ice

For the sea ice projections 13 models were used, since the required data for 6 of the 19 weighted models were not available (Table 1). The weighting scheme used in this paper does not include sea ice due to missing data in some of the models. However, it was found that including sea-ice concentration in the weighting procedure did not significantly change the relative model weights of the models for which this was possible.

Changes over the 21st century show the annual average total sea-ice area is projected to decrease by $2.6 \pm 0.73 \times 10^6$ km^2, which is a decrease of $33 \pm 9\%$. *Arzel et al.* [2006] assessed different measures of sea ice amount using a different subset of 15 of the CMIP3 models to give projected 21st century deceases of 34% for sea-ice volume and 24% for sea-ice extent. Most of the ice retreat occurs for winter and spring when the sea ice extent is largest (Figure 8). In the summer and autumn the main region of decrease is in the Weddell Sea.

Weighting the projected changes does not change the ensemble mean, but it does reduce the standard deviation of the inter-model spread by 20%, from 0.91×10^6 km^2 to 0.73×10^6 km^2. For summer and autumn the sea ice retreat around East Antarctica is larger in the weighted ensemble compared to the unweighted (Figure 9 (a) and (b)), which is consistent with less sea ice formation as the coastal easterlies decrease more in the weighted ensemble. Since the CMIP3 models are coupled it is difficult to determine the extent to which the winds force the sea ice changes and vice versa. Other differences between the weighted and unweighted ensemble that are less clearly consistent with winds changes can be seen in Figure 9. For example, the consistently weaker sea-ice retreat in the eastern Ross Sea in the weighted ensemble. The reasons for these other differences were not investigated here.

4.3. Temperature

Data for all 19 of the weighted models were available for assessment of temperature changes. Surface (skin temperature) warming over the continent is projected to be 0.34 ± 0.10°C dec^{-1} (0.32 ± 0.10°C dec^{-1} without weighting) (Figure 10). This warming is about the same magnitude as the surface warming over other large land regions around the globe. Due to the retreat of the sea-ice edge, the largest warming occurs during the winter over the marginal ice zone (MIZ), e.g. 0.51 ± 0.26°C dec^{-1} off East Antarctica (Table 4). The annual ensemble mean warming rate at 500 hPa of 0.28 °C dec^{-1} is slightly smaller than the surface warming, with no evidence of a mid-tropospheric maximum of warming, which has been observed over the last 30 years [*Turner et al.*, 2006].

The more rapid retreat of sea ice around East Antarctica in the weighted ensemble leads to larger surface warming off the coast (Figure 11), particularly in autumn and winter (Table 4). This difference is rather small in both seasons relative to the large inter-model spread in the marginal ice zone, but most significant in the autumn where the increase is larger by 35% of one standard deviation of the inter-model spread compared to 23% for summer (Table 4).

4.4. Precipitation

Data for 18 of the 19 weighted models were available for assessment of net precipitation (P-E) changes (Table 1). There is a projected increase of P-E averaged over the continent of 2.9 ± 1.2 mm a^{-1} dec^{-1} (2.9 ± 1.5 mm a^{-1} dec^{-1} without weighting); when integrated over the 21st century this represents an increase of 20% on current conditions as simulated by the CMIP3 models. This increase is a consequence of the warmer and more humid atmosphere that will transport moisture more effectively to high latitudes [*Noone and Simmonds*, 2002]. Although weighting does not significantly change the ensemble mean trend, it does reduce the standard deviation of the inter-model spread by 20%.

The surface mass balance over Antarctica has a strong influence on sea level, with an annual water turnover of 6 mm sea level equivalent [*Budd*, 1991]. In terms of sea level rise, the weighted ensemble mean P-E projection represents a negative contribution of $1.04 \pm .43$ mm a^{-1} by the year 2100.

Precipitation trends show a large spatial and seasonal variation. Absolute increases of precipitation over the continent are largest near to the coast and increases relative to current climate are largest (up to 25%) over the interior region of East Antarctica (Figure 12). Over marine regions south of 60°S (both ice free and ice covered) the annual precipitation accumulation is projected to increase at 10.2 ± 3.8 mm a^{-1} dec^{-1} (8.8 ± 3.5 mm a^{-1} dec^{-1} without weighting). This trend is largest in the autumn with 13.7 ± 4.6 mm a^{-1} dec^{-1} projected (11.3 ± 4.5 mm a^{-1} dec^{-1} without weighting). The larger precipitation increases around Antarctica in autumn in the weighted ensemble are consistent with the larger autumn increase in SAO indices and the associated contraction and strengthening of the storm track.

5. Discussion

This paper presents a broad assessment of 21st century Antarctic climate change. The CMIP3 database was used, which comprises climate model output submitted for the International Panel on Climate Change (IPCC) Assessment Report Four (AR4). In view of the large biases that some of the models produce over Antarctica, the CMIP3 model projections were weighted according the models' ability to reproduce the climate of the late 20th century [see *Connolley and Bracegirdle*, 2007].

Over the 21st century the circumpolar westerlies around Antarctica are projected to increase in magnitude in association with a poleward shift and strengthening of the storm tracks [*Lambert and Fyfe*, 2006]. This change is associated with an increasingly positive polarity of the southern annular mode (SAM), as documented by *Miller et al.* [2006]. Here we provide further dynamical insight by showing that a seasonal cycle of the westerly wind increases around Antarctica is consistent with a change in the semi-annual oscillation (SAO). Twenty-first century changes to both winds at ~60S and SAO indices show a maximum in autumn and a minimum in spring.

The change seen in the SAO indices is part of year-round increases of meridional temperature gradient that shift north of the SAO region for much of the year. These changes of temperature gradient have been linked to a poleward shift of the southern hemisphere mid-latitude storm tracks by *Yin* [2005]. There is a strong inter-model consensus for the poleward shift of the southern hemisphere storm tracks, which indicates strong confidence in the SAO changes attributable to storm track changes. However, the CMIP3 models simulate too small a spring peak of the SAO [*Raphael and Holland*, 2006], with a smaller than observed 65S to 50S temperature gradient in that season both with and without application of the weighting scheme. The reasons for this are not clear and require further investigation.

Increases of the mid-latitude meridional temperature gradient at 500 hPa are approximately 30% larger in the weighted ensemble mean compared to the simple unweighted mean. This has important implications for a number of meteorological parameters over Antarctica, mainly in autumn when the increase of temperature gradient occurs at higher latitudes and influences the SAO. The weighted ensemble for autumn shows 18% larger increases of the circumpolar westerlies at ~60S, which in summer and autumn occur sufficiently far south to be manifested as a reduction of the magnitude of coastal easterlies in large parts of coastal Antarctica. The reduced coastal easterlies are consistent with stronger sea ice retreat and associated skin temperature increases. Precipitation rate increases are 22% larger over the seas surrounding Antarctica probably due to stronger cyclonic activity in response to larger meridional temperature gradient increases.

These differences that emerge from application of the weighting scheme have consequences for aspects of Antarctic climate that are particularly important globally. The stronger winds at high latitudes will contribute to changes of the Weddell Sea gyre, which plays an important role in global ocean circulation. Increased sea-ice loss and larger warming along coastal East Antarctica may contribute to sea level rise. Warming can induce the break up of ice shelves, which has been observed to coincide with the acceleration of nearby glacier export into the ocean [*Rignot et al.*, 2005].

This is currently a key subject of research since ice-sheet dynamics are not included in the CMIP3 models.

For Antarctica as a whole the implementation of the weighting reduces the inter-model spread of annual mean sea ice retreat and P-E increase by approximately 20%, although in both cases the ensemble mean is not changed. Too few ensemble members were available for assessment to be confident that this reduction of spread was not by chance. Indeed for temperature and winds the inter-model spread was not changed. This contrasts with *Murphy et al.* [2004] and *Schmittner et al.* [2005], who found a distinct decrease of inter-model spread. One contributing factor to this may be that the ability of the CMIP3 models to correctly simulate the response of SH circulation to stratospheric ozone changes in the late 20th century would not have been captured in the weighting scheme, which uses mean climate conditions. Another important factor may be the performance of the ocean components of the models, which is difficult to assess in the absence of extensive ocean observations.

A more fundamental limitation of the method used in this analysis is that the ability of a climate model to represent current climate conditions does not necessarily indicate that the model's response to scenario forcing will be realistic. Determining which model parameters are most important for climate projection remains an open research question. As a result the methods employed by *Connolley and Bracegirdle* [2007] and others [e.g. *Murphy et al.*,2004; *Tebaldi et al.*, 2004] require a number of subjective choices. Despite these issues, the weighting procedure is potentially useful for highlighting the key physical processes responsible for differences between the weighted and unweighted ensemble, which can then be assessed for possible systematic failings.

One example that requires further research is the reason for the more strongly weighted models producing larger increases of meridional temperature gradient. One possibility is that the models with larger weights possess a more realistic representation of the effect of convection on the vertical temperature profile of the troposphere. One indicator of this is that the difference between the weighted and unweighted ensemble mean temperature trend increases with increasing height in regions where convection dominates the atmospheric vertical profile north of the main SH storm track [*Frierson*, 2006]. Whereas this is not evident at higher latitudes, where convection is less important for determining the vertical tropospheric temperature profile.

ACKNOWLEDGEMENTS

We acknowledge the modelling groups for making their simulations available for analysis, the Program for Climate Model Diagnosis and Inter-comparison (PCMDI) for collecting and archiving the CMIP3 model output, and the WCRP's Working Group on Coupled Modelling (WGCM) for organizing the model data analysis activity. The WCRP CMIP3 multi-model data set is supported by the Office of Science, U.S. Department of Energy.

6. Tables

Table 1. Models used in this study. Models for which monthly mean data were successfully downloaded and processed for projections of each variable are indicated in the 'Variable' columns. Skin temperature is denoted by 'ts', total precipitation rate by 'pr', surface latent heat flux by 'hfls', u and v component of the near-surface wind vector by 'uvas' and sea ice concentration by 'sic'.

Model ID	Weight	Institute	Variable				
			ts	pr	hfls	uvas	sic
MPI ECHAM5	0.42	Max Planck Institute for Meteorology - Germany	×	×	×	×	×
CCCMA CGCM3	0.31	Canadian Centre for Climate Modelling and Analysis - Canada	×	×	×	×	×
UKMO HadGEM1	0.30	Met Office's Hadley Centre for Climate Prediction - UK	×	×	×	×	×
UKMO HadCM3	0.27	Met Office's Hadley Centre for Climate Prediction - UK	×	×	×	×	×
MIROC(hires)	0.19	Center for Climate System Research - Japan	×	×	×	×	
NCAR CCSM3	0.14	National Center for Atmospheric Research - USA	×	×	×		
CSIRO Mk3	0.13	Commonwealth Scientific and Industrial Research Organisation (CSIRO) Atmospheric Research - Australia	×	×	×		×
GFDL CM2.1	0.11	Geophysical Fluid Dynamics Laboratory – USA	×	×	×	×	
MRI CGCM2	0.10	Meteorological Research Institute - Japan	×	×	×	×	×
NCAR PCM1	0.10	National Center for Atmospheric Research - USA	×	×	×		
MIROC(medres)	0.09	Center for Climate System Research - Japan	×	×	×	×	×
IPSL CM4	0.08	Institut Pierre Simon Laplace - France	×	×	×		×
INM CM3	0.07	Institute for Numerical Mathematics - Russia	×	×	×	×	×
GISS ER	0.07	Goddard Institute for Space Studies - USA	×	×		×	×
CNRM CM3	0.07	Center National de Recherches Meteorologiques - France	×	×	×	×	×
GFDL CM2.0	0.06	Geophysical Fluid Dynamics Laboratory - USA	×	×	×	×	
BCCR BCM2	0.03	Bjerknes Center for Climate Research - Norway	×	×	×	×	×
GISS EH	0.00	Goddard Institute for Space Studies - USA	×		×	×	
IAP FGOALS1	0.00	Institute for Atmospheric Physics - China	×	×	×	×	×

Table 2. Ensemble mean and inter-model standard deviation of mean monthly wind vector magnitude averaged over coastal East Antarctica (the region is shown in Figure 7d and extends over 0° to 150° in longitude and –65.0° to –70.0° in latitude). Percentage difference between the 2080-2099 mean and the 2004-2023 mean with weighted absolute change in brackets.

Season	Weighted change	Unweighted change
Spring	0% (0.0m/s) ± 4%	0% ± 4%
Summer	-7% (-0.3m/s) ± 6%	-4% ± 7%
Autumn	-5% (-0.3m/s) ± 5%	-3% ± 4%
Winter	0% (0.0m/s) ± 4%	-1% ± 4%

Table 3. As in Table 2, but for coastal West Antarctica (the region is shown in Figure 7d and extends over -140° to -80° in longitude and –70° to -75° in latitude).

Season	Weighted trend	Unweighted trend
Spring	-3% (-0.1m/s) ± 5%	-1% ± 6%
Summer	-7% (-0.2m/s) ± 5%	-6% ± 5 %
Autumn	-5% (-0.2m/s) ± 6%	-4% ± 7%
Winter	0% (0.0m/s) ± 7%	-2% ± 6%

Table 4. Ensemble mean and inter-model spread of skin temperature change around 0° meridian (315° to 80° longitude and marine regions south of –62.5° in latitude). Difference between the 2080-2099 mean and the 2004-2023 mean divided by 7.7 to show change in °C per decade.

Season	Weighted trend °C dec^{-1}	Unweighted trend °C dec^{-1}
Spring	0.29 ± 0.16	0.27 ± 0.18
Summer	0.15 ± 0.09	0.14 ± 0.09
Autumn	0.36 ± 0.17	0.30 ± 0.17
Winter	0.51 ± 0.26	0.45 ± 0.26
Annual	0.33 ± 0.16	0.29 ± 0.16

7. Figure captions

Figure 1: 21st century near-surface (10m) westerly wind component change for (a) DJF, (b) MAM, (c) JJA and (d) SON. Difference between 2080-2099 mean and 2004-2023 mean. Calculated from monthly mean wind vectors. The hatched regions show grid points where the changes are significant (larger than one standard deviation of the inter-model spread at that grid point).

Figure 2. Difference between zonal mean sea level pressure (SLP) at 50S and 65S. (a) Mean for 2004-2023 (thick solid line) and 2080-2099 (dashed line). The thin solid lines show the standard deviation of the inter-model spread of SAO for the 2004-2023 period. (b) The projected change over the 21st century (2080-2099 mean minus 2004-2023 mean). The solid (dotted) lines show the weighted (unweighted) ensemble statistics. The ensemble mean is indicated by thick lines and standard deviation of the inter-model spread by thin line lines.

Figure 3: As in Figure 2, but for 500 hPa temperature (T500).

Figure 4: 21st century change of the 500 hPa meridional temperature gradient (the 2080-2099 mean minus the 2004-2023 mean) for (a) weighted and (b) unweighted ensemble mean. The contour intervals are 0.2 °C per 1000 km; solid lines show changes greater than or equal to zero and dashed lines show negative changes.

Figure 5: 500 hPa temperature. Difference between 2080-2099 mean and 2004-2023 mean for (a) 50S and (b) 65S. The solid (dotted) lines show the weighted (unweighted) ensemble statistics. The ensemble mean is indicated by thick lines and standard deviation of the inter-model spread by thin line lines.

Figure 6: As in Figure 4a, but for skin temperature.

Figure 7: As in Figure 1, but for monthly-mean wind vector magnitude. The hatched regions show grid points where the changes are significant (larger than one standard deviation of the inter-model spread at that grid point). The regions used for the calculations in Table 2 and Table 3 are shown delimited by a solid line (coastal East Antarctica) and dashed line (coastal West Antarctica).

Figure 8: As in Figure 1, but for sea ice concentration.

Figure 9: Difference between weighted and unweighted ensemble mean sea ice concentration projected 21st century change (2080-2099 minus 2004-2023 mean) for (a) DJF, (b) MAM, (c) JJA and (d) SON.

Figure 10: As in Figure 1, but for skin temperature. The changes are significant (larger than one standard deviation of the inter-model spread) at almost all grid points, therefore the hatching used in Figure 1 and Figure 7 is omitted here.

Figure 11: As in Figure 9, but for skin temperature.

Figure 12: Weighted ensemble mean 21st century change of annual mean precipitation rate. Difference between 2080-2099 mean and 2004-2023 mean. (a)

Absolute change in mm/a and (b) percentage change compared to 2004-2023 mean. The changes are significant (larger than one standard deviation of the inter-model spread) at almost all grid points, therefore the hatching used in Figure 1 and Figure 7 is omitted here.

8. References

Arzel, O., T. Fichefet, and H. Goosse (2006), Sea ice evolution over the 20th and 21st centuries as simulated by current AOGCMs, *Ocean Model., 12*, 401-415, doi:10.1016/j.ocemod.2005.08.002.

Budd, W. F. (1991), Antarctica and global change, *Clim. Change, 18*, 271-299, doi:10.1007/BF00139002.

Carril, A. F., C. G. Menendez, and A. Navarra (2005), Climate response associated with the Southern Annular Mode in the surroundings of Antarctic Peninsula: A multimodel ensemble analysis, *Geophys. Res. Lett., 32*, L16713, doi:10.1029/2005GL023581.

Connolley, W. M., and T. J. Bracegirdle (2007), An Antarctic assessment of IPCC AR4 coupled models, *Geophys. Res. Lett.*, doi:10.1029/2007GL031648, in press.

Connolley, W. M., and S. A. Harangozo (2001), A comparison of five numerical weather prediction analysis climatologies in southern high latitudes, *J. Clim., 14*, 30-44, doi:10.1175/1520-0442(2001)014<0030:ACOFNW>2.0.CO;2.

Frierson, D. M. W. (2006), Robust increases in midlatitude static stability in simulations of global warming, *Geophys. Res. Lett., 33*, L24816, doi:10.1029/2006GL027504.

Fyfe, J. C., and O. A. Saenko (2006), Simulated changes in the extratropical Southern Hemisphere winds and currents, *Geophys. Res. Lett., 33*, L06701, doi:10.1029/2005GL025332.

Giovinetto, M. B., D. H. Bromwich, and G. Wendler (1992), Atmospheric net transport of water vapor and latent heat across 70 °S, *J. Geophys. Res., 97*, 917-930.

Gong, D., and S. Wang (1999), Definition of Antarctic oscillation index, *Geophys. Res. Lett., 26*, 459-462, doi:10.1029/1999GL900003.

Gregory, J., and P. Huybrechts (2006), Ice-sheet contributions to future sea-level change, *Philos. Trans. R. Soc. A, 364*, 1709-1731 doi:10.1098/rsta.2006.1796.

Lambert, S. J., and J. C. Fyfe (2006), Changes in winter cyclone frequencies and strengths simulated in enhanced greenhouse warming experiments: results from the

models participating in the IPCC diagnostic exercise, *Clim. Dyn.*, *26*, 713-728, doi:10.1007/s00382-006-0110-3.

Lynch, A. H., P. Uotilla, and J. J. Cassano (2006), Changes in synoptic weather patterns in the polar regions in the 20th and 21st centuries, Part 2: Antarctic, *Int. J. Climatol.*, *26*, 1181-1199, doi:10.1002/joc.1305.

Marshall, G. J. (2007), Half-century seasonal relationships between the Southern Annular Mode and Antarctic temperatures, in *Int. J. Climatol.*, edited, pp. 373-383.

Meehl, G. A. (1987), The annual cycle and interannual variability in the tropical Pacific and Indian Ocean regions, *Mon. Weather Rev.*, *115*, 27-50, doi:10.1175/1520-0493(1987)115<0027:TACAIV>2.0.CO;2.

Meehl, G. A. (1991), A reexamination of the mechanism of the semiannual oscillation in the Southern Hemisphere, *J. Clim.*, *4*, 911-925, doi:10.1175/1520-0442(1991)004<0911:AROTMO>2.0.CO;2.

Meehl, G. A., J. W. Hurrell, and H. van Loon (1998), A modulation of the mechanism of the semiannual oscillation in the Southern Hemisphere, *Tellus Ser. A*, *50A*, 442-450, doi:10.1034/j.1600-0870.1998.t01-3-00005.x.

Miller, R. L., G. A. Schmidt, and D. T. Shindell (2006), Forced annular variations in the 20th century Intergovernmental Panel on Climate Change Fourth Assessment Report models, *J. Geophys. Res.*, *111*, doi:10.1029/2005JD006323.

Murphy, J. M., D. M. H. Sexton, D. N. Barnett, G. S. Jones, M. J. Webb, M. Collins, and D. A. Stainforth (2004), Quantification of modelling uncertainties in a large ensemble of climate change simulations, *Nature*, *430*, 768-772, doi:10.1038/nature02771.

Noone, D., and I. Simmonds (2002), Annular variations in moisture transport mechanisms and the abundance of delta O-18 in Antarctic snow, in *J. Geophys. Res.*, edited, p. 10.

Räisänen, J. (2007), How reliable are climate models?, *Tellus Ser. A*, *59A*, 2-29, doi:10.1111/j.1600-0870.2006.00211.x.

Raphael, M. N., and M. M. Holland (2006), Twentieth century simulation of the southern hemisphere climate in coupled models. Part 1: large scale circulation variability, *Clim. Dyn.*, *26*, 217-228, doi:10.1007/s00382-005-0082-8.

1 Rignot, E., G. Casassa, S. Gogineni, P. Kanagaratnam, W. Krabill, H. Pritchard, A.
2 Rivera, R. Thomas, J. Turner, and D. G. Vaughan (2005), Recent ice loss from the
3 Fleming and other glaciers, Wordie Bay, West Antarctic Peninsula, *Geophys. Res.*
4 *Lett., 32*, doi:10.1029/2004GL021947.

5 Schmittner, A., M. Latif, and B. Schneider (2005), Model projections of the North
6 Atlantic thermohaline circulation for the 21st century assessed by observations,
7 *Geophys. Res. Lett., 32*, L23710, doi:10.1029/2005GL024368.

8 Shindell, T., and G. A. Schmidt (2004), Southern Hemisphere climate response to
9 ozone changes and greenhouse gas increases, *Geophys. Res. Lett., 31*, L18209,
10 doi:10.1029/2004GL020724.

11 Tebaldi, C., R. l. Smith, D. Nychka, and L. O. Mearns (2005), Quantifying
12 Uncertainty in Projections of Regional Climate Change: A Bayesian Approach to the
13 Analysis of Multimodel Ensembles, *J. Clim, 18*, 1524-1540, doi:10.1175/JCLI3363.1.

14 Thompson, D. W. J., and S. Solomon (2002), Interpretation of recent Southern
15 Hemisphere climate change, *Science, 296*, 895-899, doi:10.1126/science.1069270.

16 Turner, J., T. A. Lachlan-Cope, S. R. Colwell, G. J. Marshall, and W. M. Connolley
17 (2006), Significant warming of the Antarctic winter troposphere, *Science, 311*, 1914-
18 1917, doi:10.1126/science.1121652.

19 Uppala, S. M., P. W. Kallberg, A. J. Simmons, U. Andrae, V. D. Bechtold, M.
20 Fiorino, J. K. Gibson, J. Haseler, A. Hernandez, G. A. Kelly, X. Li, K. Onogi, S.
21 Saarinen, N. Sokka, R. P. Allan, E. Andersson, K. Arpe, M. A. Balmaseda, A. C. M.
22 Beljaars, L. van de Berg, J. Bidlot, N. Bormann, S. Caires, F. Chevallier, A. Dethof,
23 M. Dragosavac, M. Fisher, M. Fuentes, S. Hagemann, E. Holm, B. J. Hoskins, L.
24 Isaksen, P. A. E. M. Janssen, R. Jenne, A. P. McNally, J. F. Mahfouf, J. J. Morcrette,
25 N. A. Rayner, R. W. Saunders, P. Simon, A. Sterl, K. E. Trenberth, A. Untch, D.
26 Vasiljevic, P. Viterbo, and J. Woollen (2005), The ERA-40 re-analysis, *Q. J. R.*
27 *Meteorol. Soc., 131*, 2961-3012, doi:10.1256/qj.04.176.

28 van den Broeke, M. R. (1998), The semi-annual oscillation and Antarctic climate. Part
29 1: Influence on near surface temperatures (1957-79), *Antarct. Sci., 10*, 175-183.

30 van den Broeke, M. R., R. S. W. van de Wal, and M. Wild (1997), Representation of
31 Antarctic Katabatic Winds in a High-Resolution GCM and a Note on Their Climate
32 Sensitivity, *J. Clim., 10*, 3111-3130, doi:10.1175/1520-
33 0442(1997)010<3111:ROAKWI>2.0.CO;2.

van Loon, H. (1967), The half-yearly oscillations in middle and high Southern latitudes and the coreless winter, *J. Atmos. Sci.*, *24*, 472-486, doi:10.1175/1520-0469(1967)024<0472:THYOIM>2.0.CO;2.

Vaughan, D. G., J. L. Bamber, M. Giovinetto, J. Russell, and A. P. R. Cooper (1999), Reassessment of net surface mass balance in Antarctica, *J. Clim.*, *12*, 933-946, doi:10.1175/1520-0442(1999)012<0933:RONSMB>2.0.CO;2.

Yin, J. H. (2005), A consistent poleward shift of the storm tracks in simulations of 21st century climate, *Geophys. Res. Lett.*, *32*, L18701, doi:10.1029/2005GL023684.

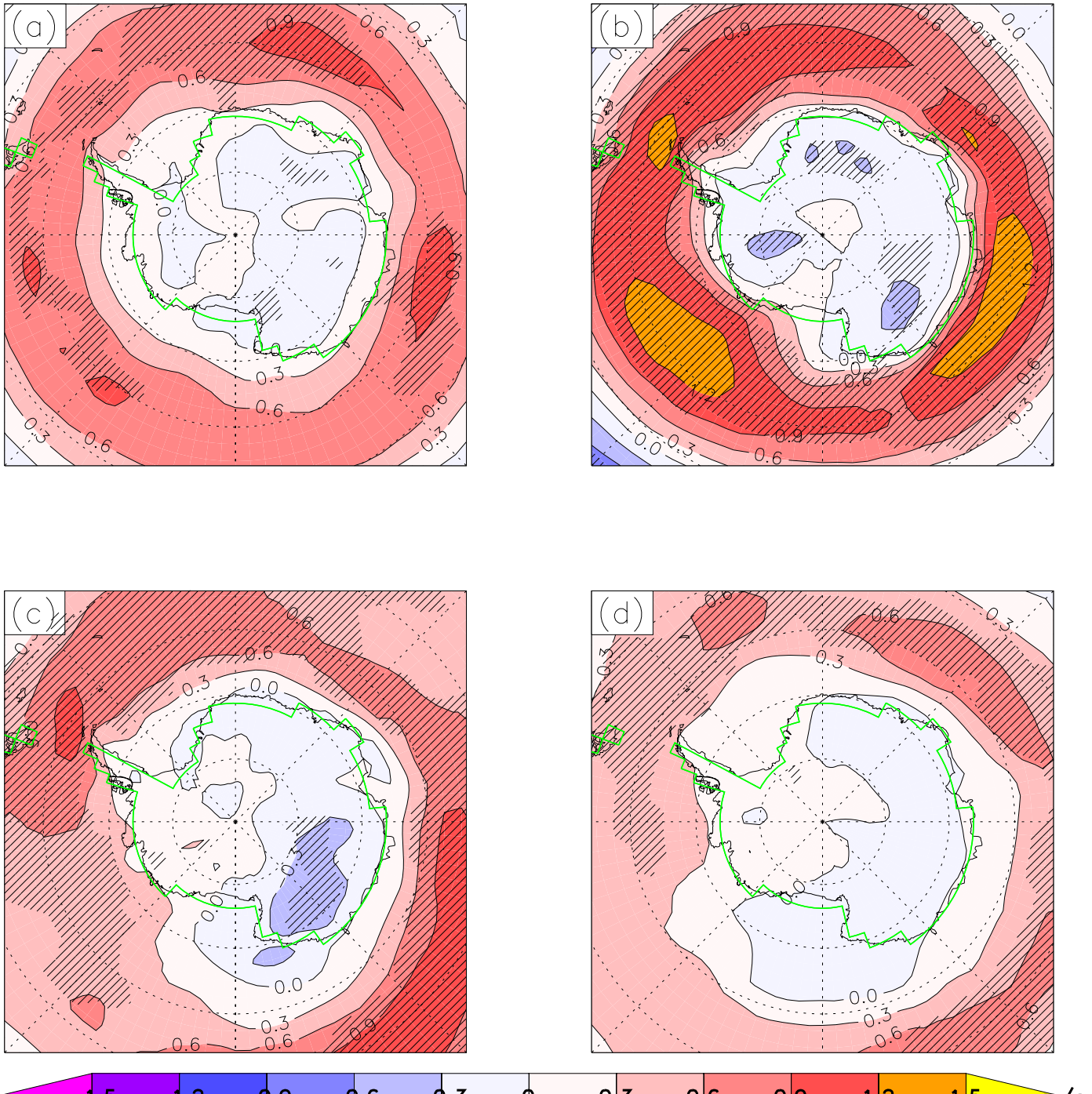
(a)
(b)
(c)
(d)
−1.5
−1.2
−0.9
−0.6
−0.3
0
0.3
0.6
0.9
1.2
1.5
m/s

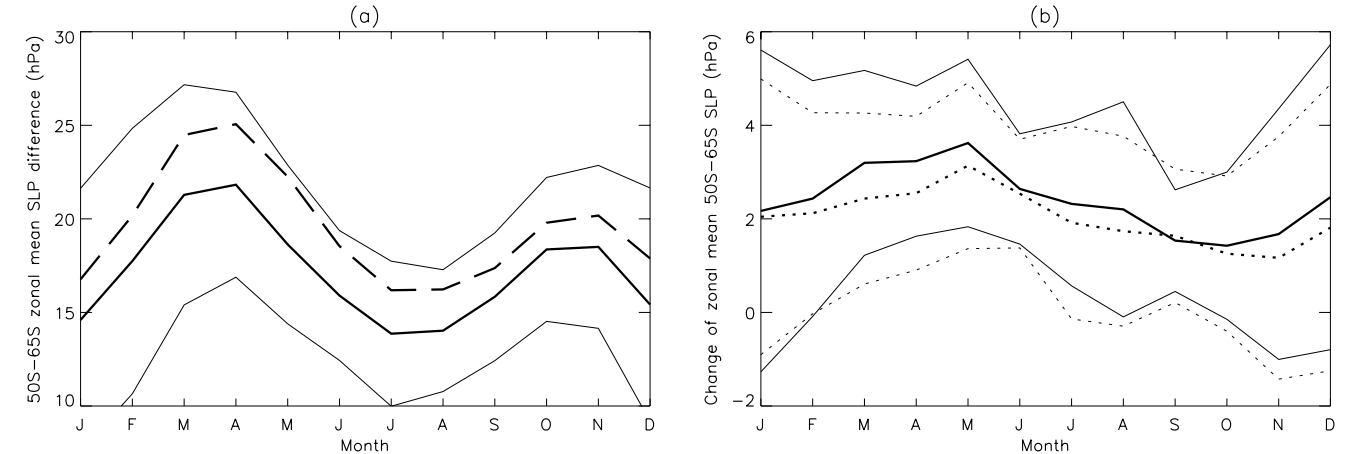
(a)
50S–65S zonal mean SLP difference (hPa)
30
25
20
15
10
J F M A M J J A S O N D
Month
(b)
Change of zonal mean 50S–65S SLP (hPa)
6
4
2
0
−2
J F M A M J J A S O N D
Month

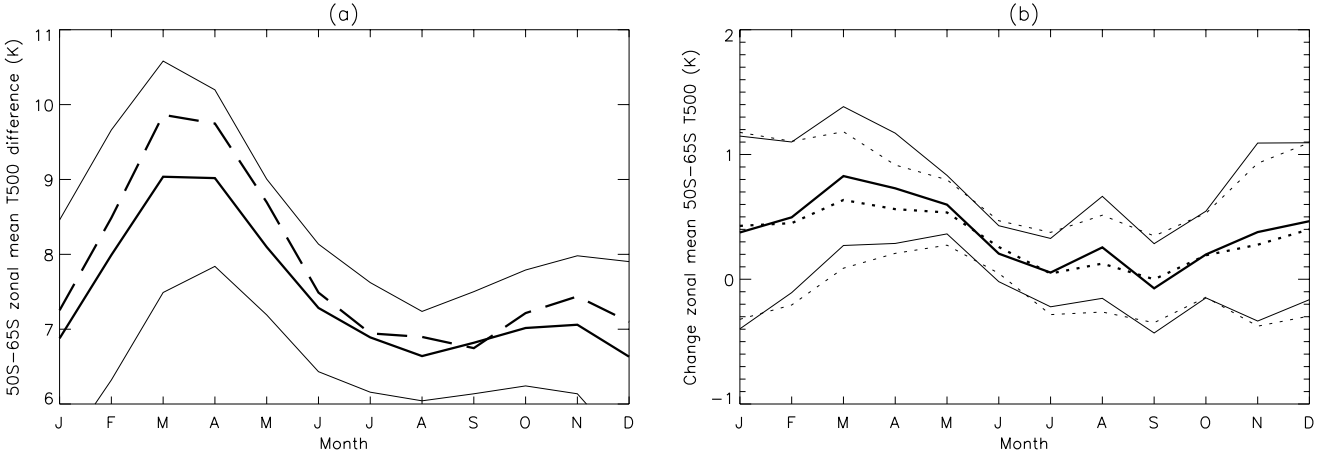
(a)
50S–65S zonal mean T500 difference (K)
11
10
9
8
7
6
J F M A M J J A S O N D
Month
(b)
Change zonal mean 50S–65S T500 (K)
2
1
0
−1
J F M A M J J A S O N D
Month

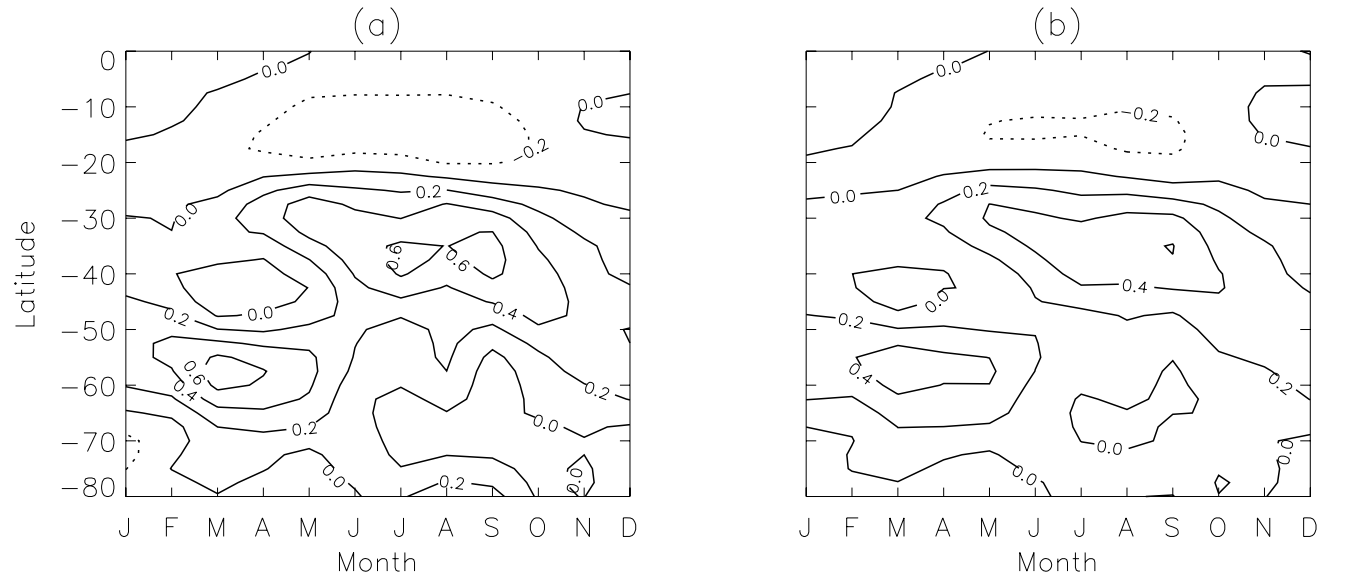
(a)
(b)
Latitude
0
−10
−20
−30
−40
−50
−60
−70
−80
J F M A M J J A S O N D
Month
J F M A M J J A S O N D
Month
0.0
0.2
0.4
0.6

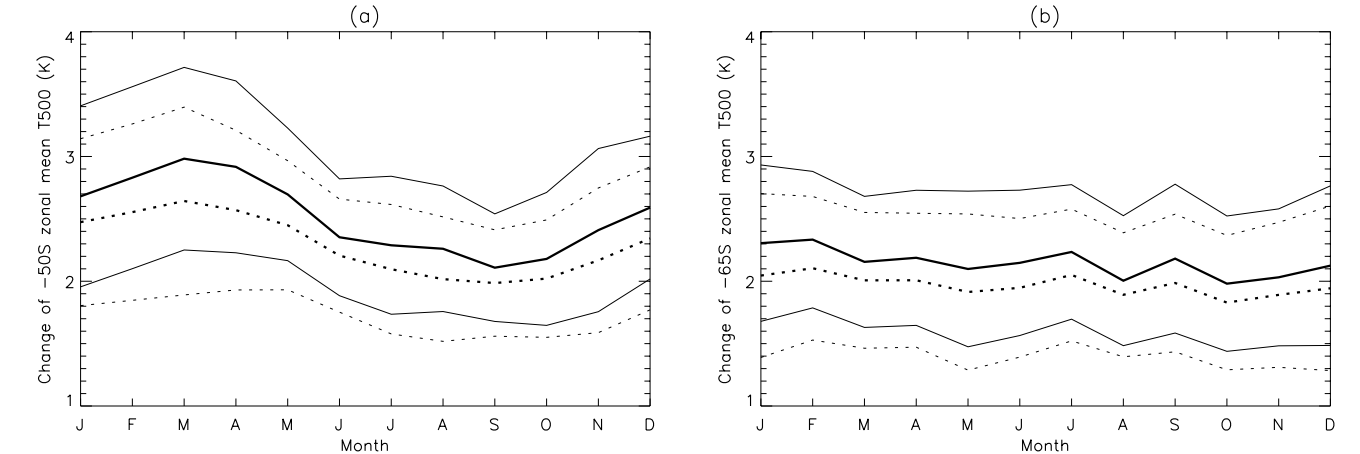
(a)
Change of −50S zonal mean T500 (K)
4
3
2
1
J
F
M
A
M
J
J
A
S
O
N
D
Month
(b)
Change of −65S zonal mean T500 (K)
4
3
2
1
J
F
M
A
M
J
J
A
S
O
N
D
Month

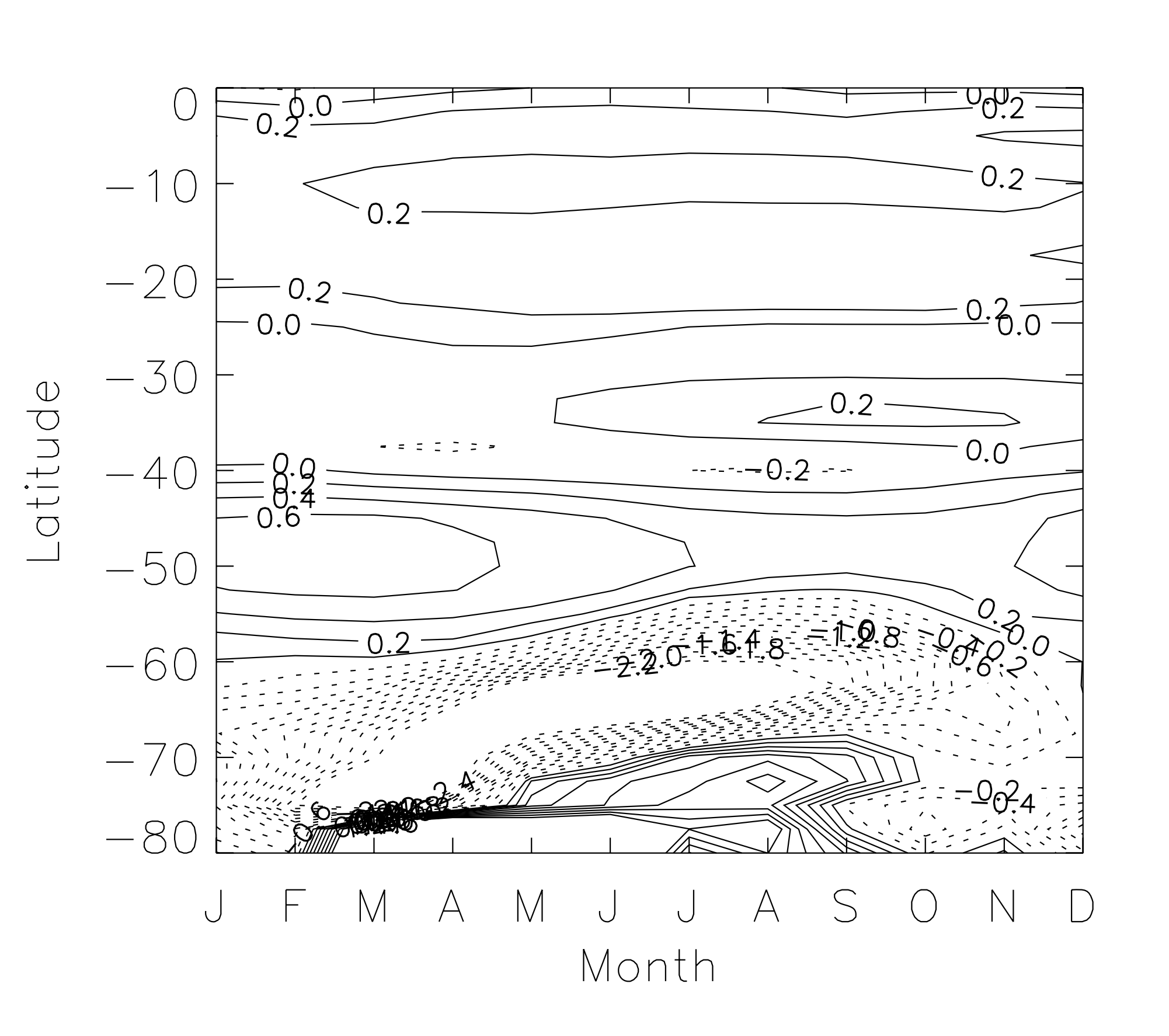
0
−10
−20
−30
−40
−50
−60
−70
−80
Latitude
J
F
M
A
M
J
J
A
S
O
N
D
Month
0.0
0.2
0.4
0.6
−0.2
−0.4
−0.6
−0.8
−1.0
−1.2
−1.4
−1.6
−1.8
−2.0
−2.2

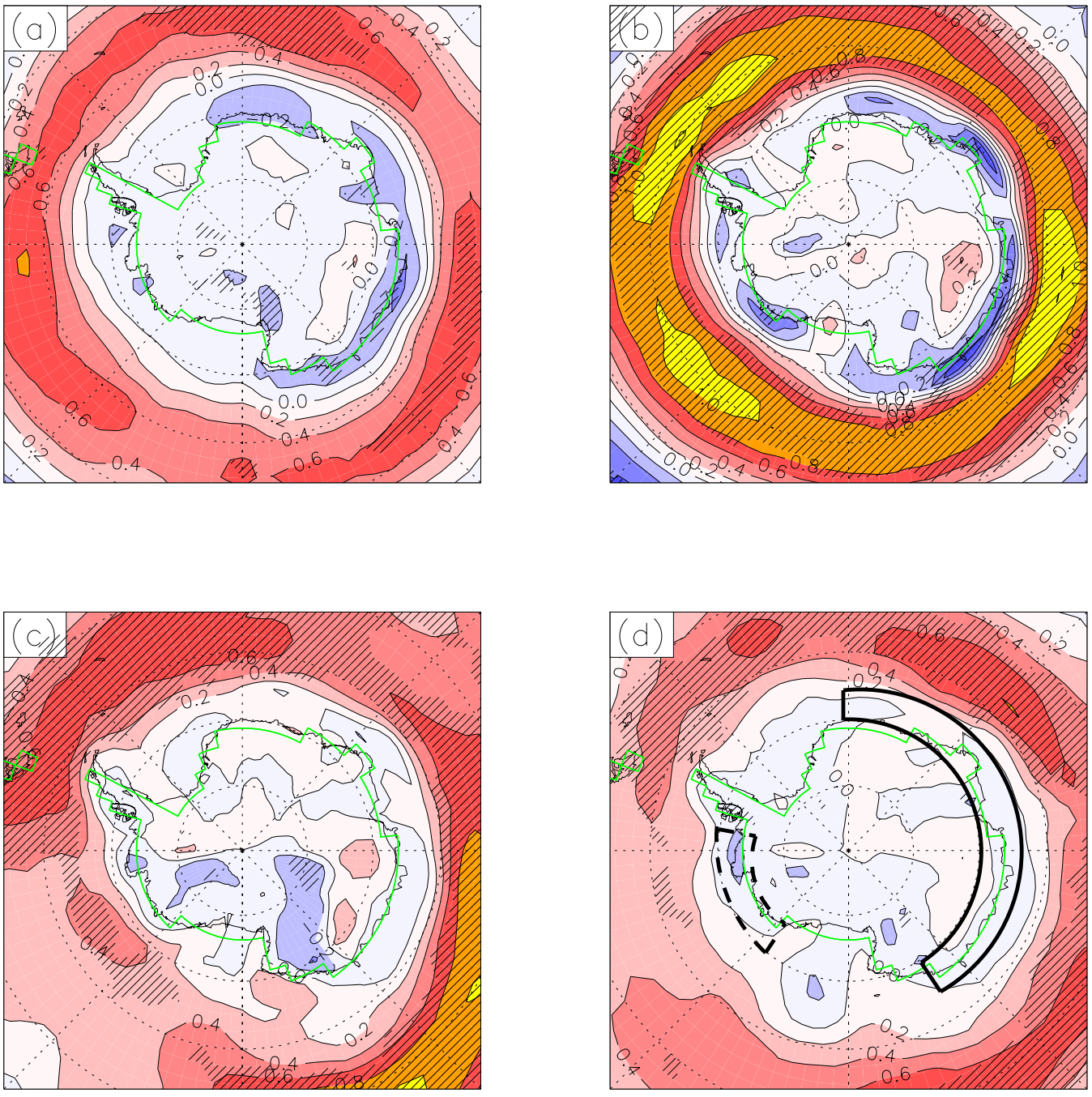
(a)
(b)
(c)
(d)
−1
−0.8
−0.6
−0.4
−0.2
0
0.2
0.4
0.6
0.8
1
m/s

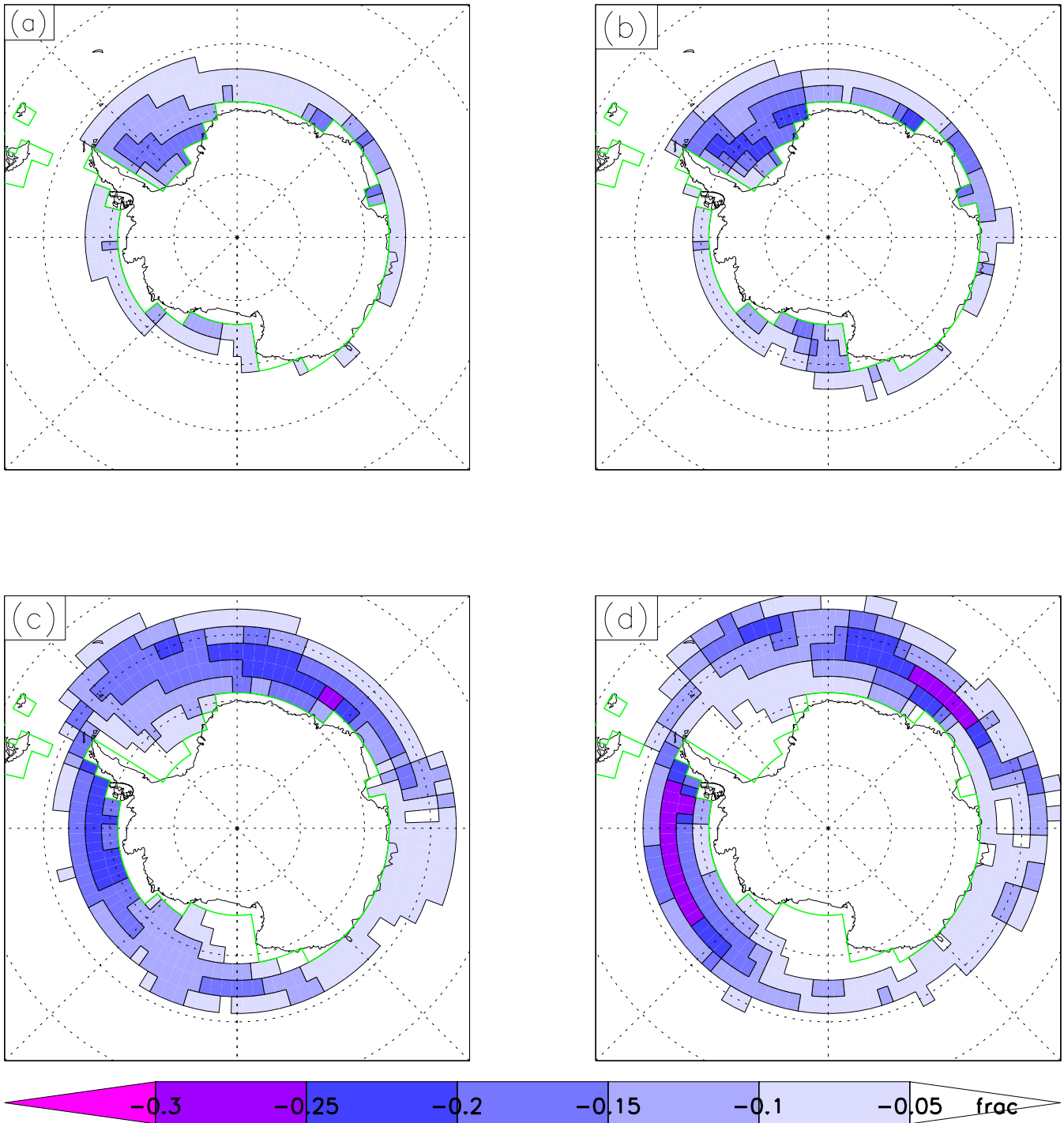
(a)
(b)
(c)
(d)
−0.3
−0.25
−0.2
−0.15
−0.1
−0.05
frac

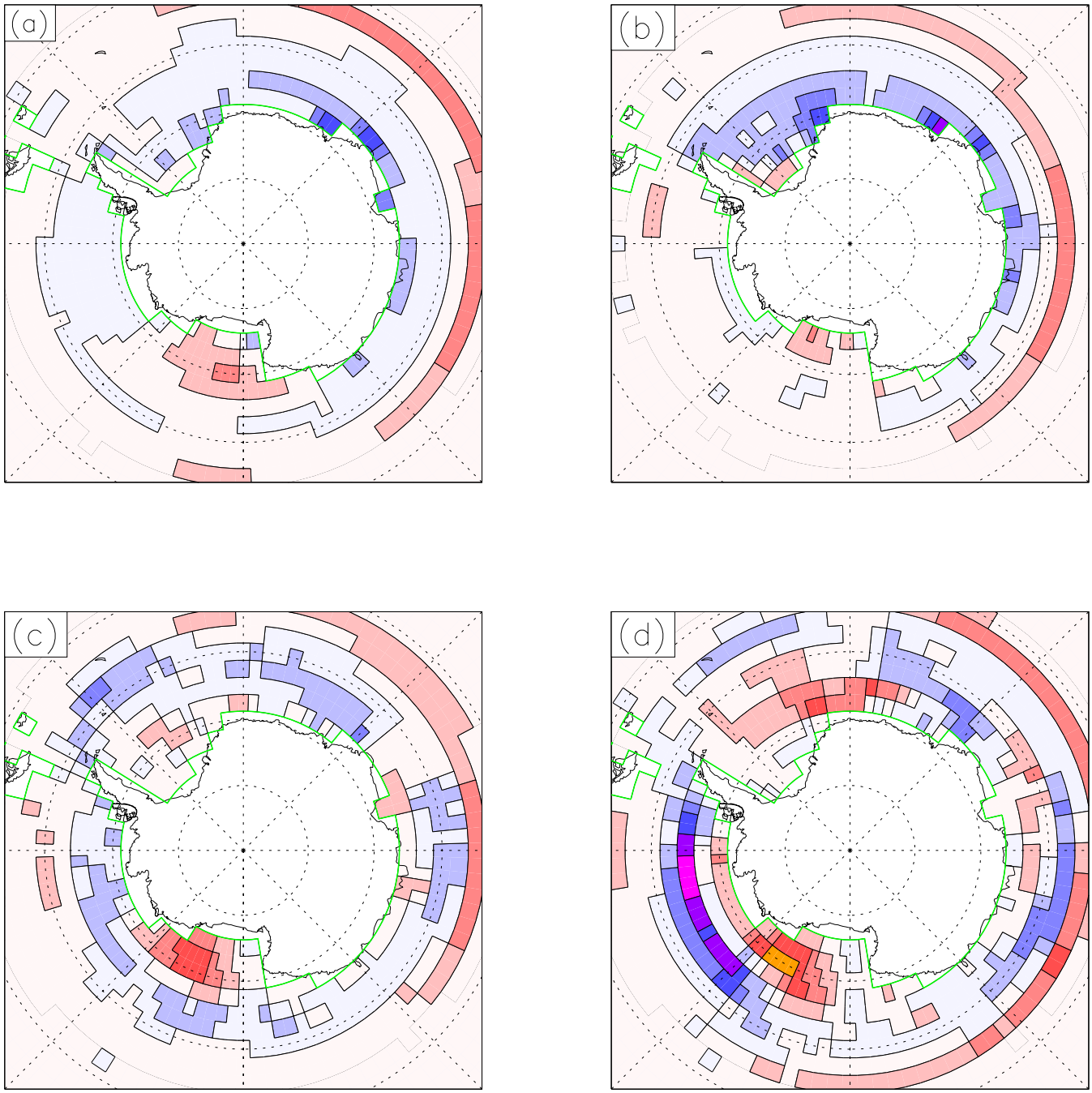
(a)
(b)
(c)
(d)
−0.1
−0.08
−0.06
−0.04
−0.02
0
0.02
0.04
0.06
0.08
0.1
frac

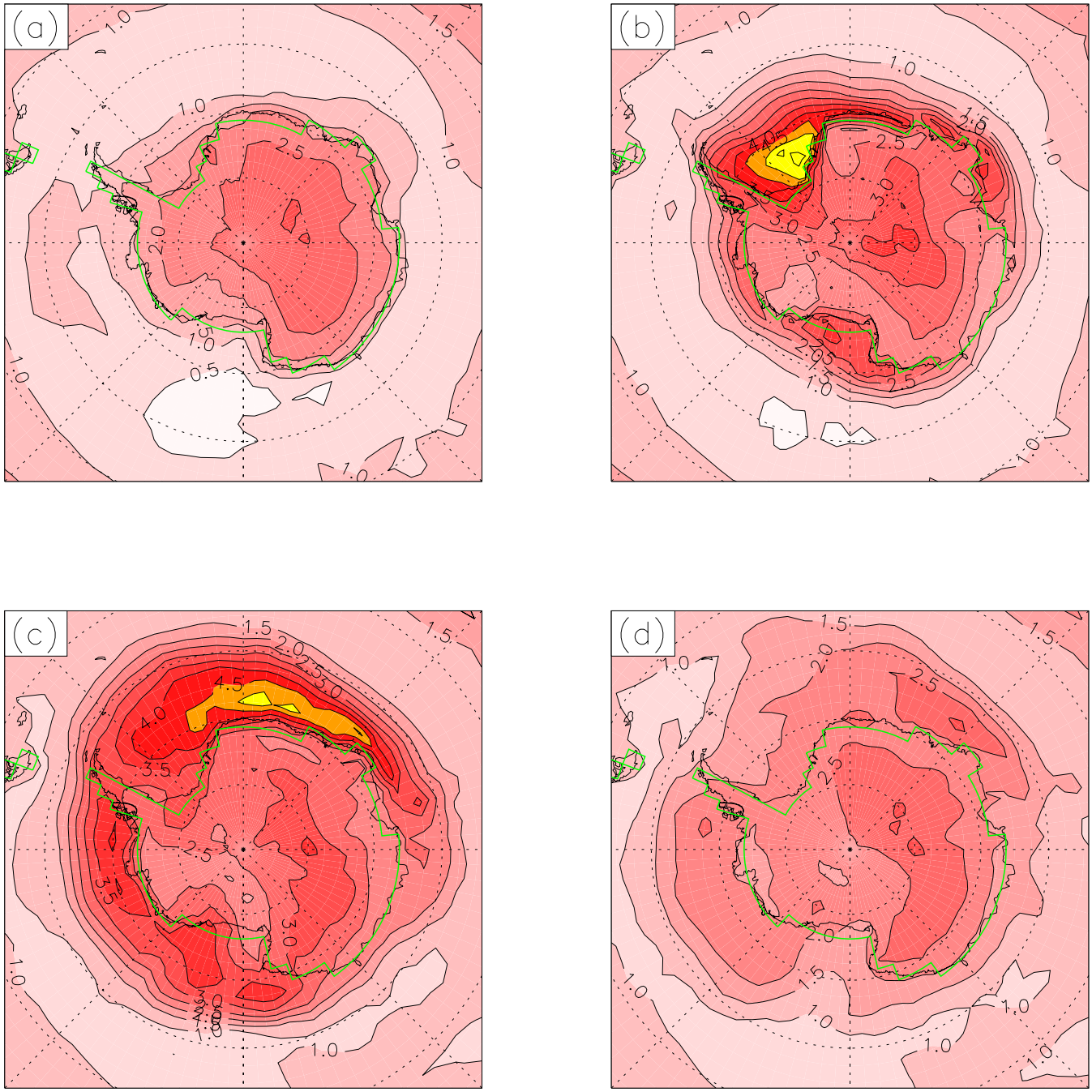
(a)
(b)
(c)
(d)
0
0.5
1
1.5
2
2.5
3
3.5
4
4.5
5 °C

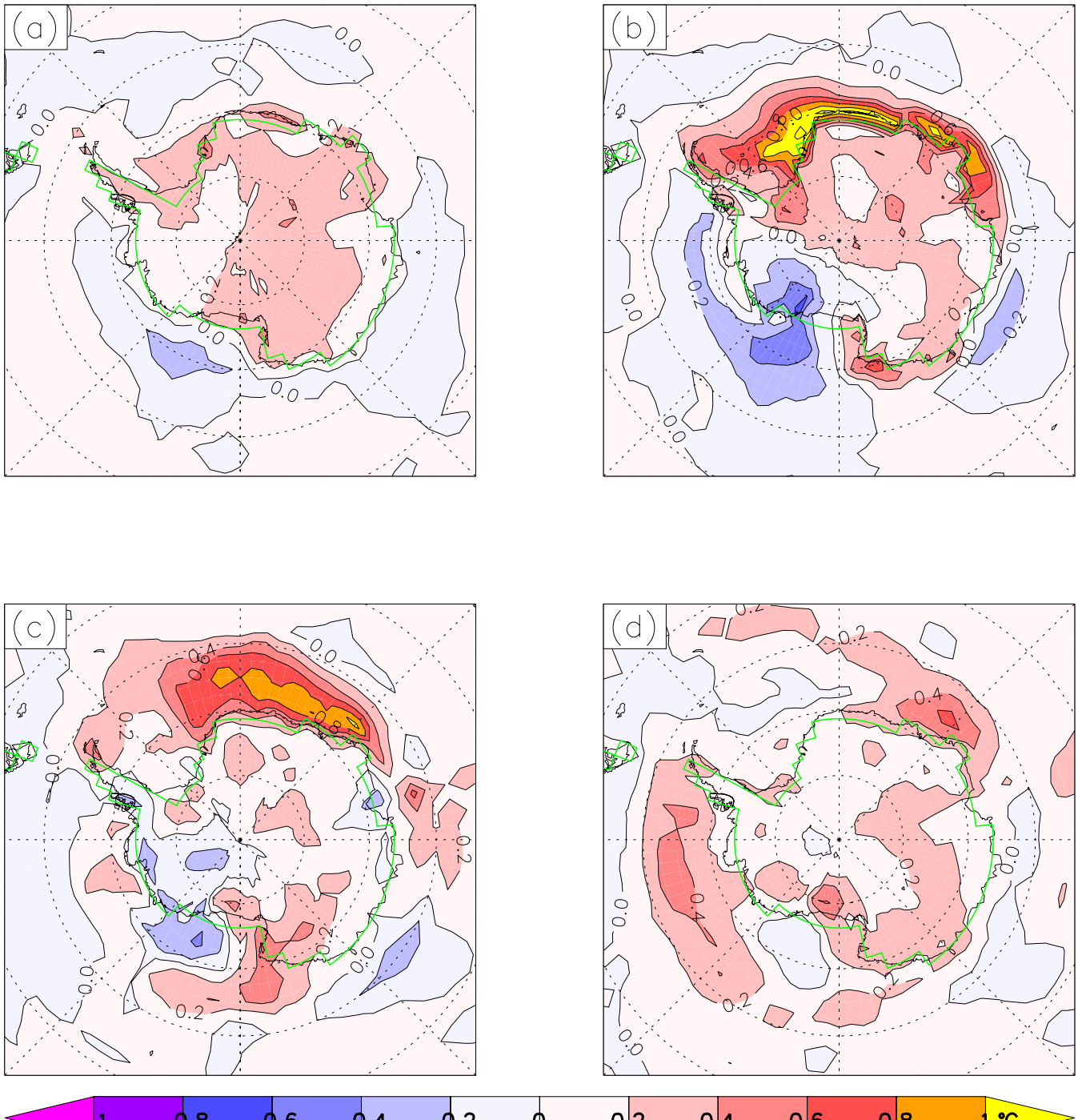
(a)
(b)
(c)
(d)
−1
−0.8
−0.6
−0.4
−0.2
0
0.2
0.4
0.6
0.8
1 °C

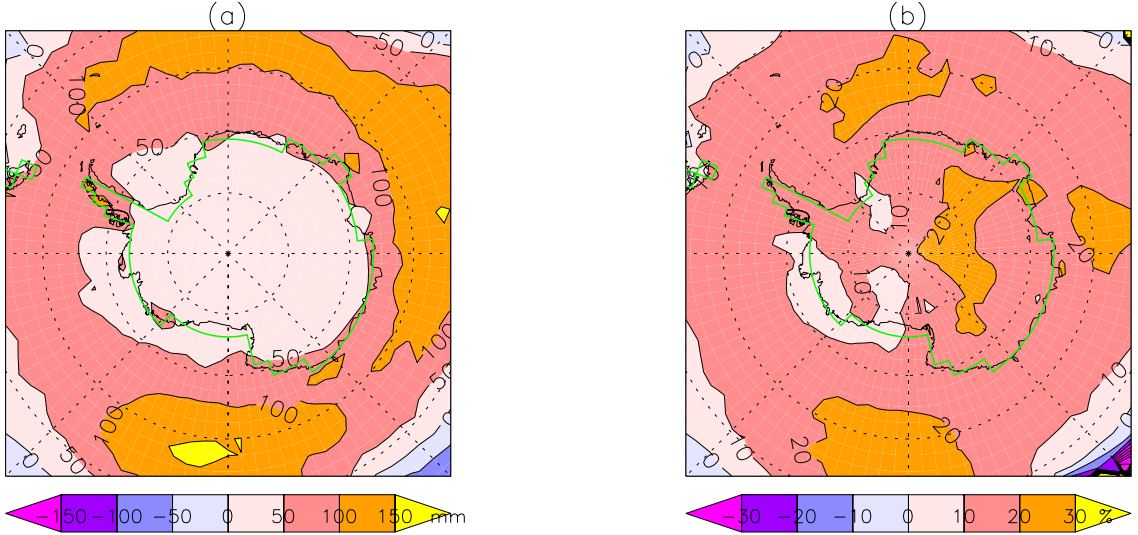
(a)
(b)
−150 −100 −50 0 50 100 150 mm
−30 −20 −10 0 10 20 30 %